The Innate Growth Bistability and Fitness Landscapes of Antibiotic-Resistant Bacteria

J. Barrett Deris *et al.*

Science **342**, (2013);
DOI: 10.1126/science.1237435

Science (print ISSN 0036-8075; online ISSN 1095-9203) is published weekly, except the last week in December, by the American Association for the Advancement of Science, 1200 New York Avenue NW, Washington, DC 20005.

The Innate Growth Bistability and Fitness Landscapes of Antibiotic-Resistant Bacteria

J. Barrett Deris, Minsu Kim, Zhongge Zhang, Hiroyuki Okano, Rutger Hermsen, Alexander Groisman, Terence Hwa*

READ THE FULL ARTICLE ONLINE
http://dx.doi.org/10.1126/science.1237435

Cite this article as J. B. Deris *et al.*, *Science* **342**, 1237435 (2013).
DOI: 10.1126/science.1237435

Introduction: Understanding how bacteria harboring antibiotic resistance grow in the presence of antibiotics is critical for predicting the spread and evolution of drug resistance. Because drugs inhibit cell growth and a cell's growth state globally influences its gene expression, the expression of drug resistance is subject to an innate, growth-mediated feedback, leading to complex behaviors that affect both the characterization and the prevention of antibiotic resistance. We characterized the consequences of this feedback for the growth of antibiotic-resistant bacteria.

Methods: We studied the growth of *Escherichia coli* strains expressing resistance to translation-inhibiting antibiotics, by using both bulk and single-cell techniques. The growth of each strain was quantified in a broad range of drug concentrations by using time-lapse microscopy (to track the responses of individual cells to antibiotics inside a microfluidic chemostat) and by the enrichment of batch cultures for nongrowing cells. We formulated a quantitative phenomenological model to predict the growth rates of drug-resistant strains in the presence of drugs, based on the well-characterized biochemistry of drug and drug-resistance interactions and on bacterial growth laws that dictate relations between cell growth and gene expression. We tested the model predictions for various drugs and resistance mechanisms by constructing strains that constitutively express varying degrees of drug resistance.

Results: In strains expressing a moderate degree of drug resistance, growth rates dropped abruptly above a critical drug concentration, the minimum inhibitory concentration (MIC), whose value increased linearly with the basal level of resistance expression (see figure below, panel A). Cells exhibited growth bistability over a broad range of drug concentrations below the MIC: Isogenic cells expressing drug resistance coexisted in growing and nongrowing states in a homogeneous environment (panel B). Our model accurately predicted the range of drug concentrations in which growth bistability occurred, as well as the growth rates of the growing subpopulation, without any ad hoc fitting parameters. These findings reveal a plateau-like fitness landscape (panel A), which can be used to study the evolution of drug resistance in environments with varying drug concentrations.

Discussion: The broad occurrence of growth bistability in drug-resistant bacteria challenges the common notions and measures of drug efficacy and resistance. And because growth bistability can arise without complex regulation when gene expression is coupled to the state of cell growth, similar physiological links may underlie the growth bistability implicated in causing bacterial persistence. The availability of quantitative, predictive models will facilitate the formulation of strategies to limit the efficacy and evolvability of drug resistance.

FIGURES IN THE FULL ARTICLE

SUPPLEMENTARY MATERIALS

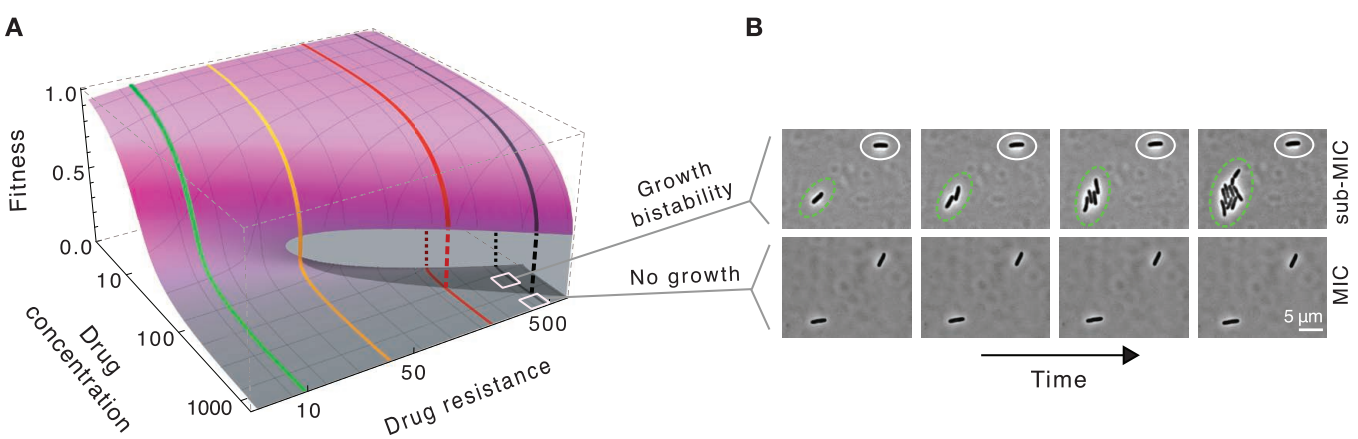

Fitness landscape and growth bistability. (**A**) This fitness landscape describes the fitness, or growth rates, of bacterial strains exposed to antibiotics (colored lines indicate the fitness of four example strains). Fitness drops abruptly at high drug concentrations. The shaded area shows a broad region of growth bistability, throughout which we observe that genetically identical cells possessing drug resistance are split into subpopulations of growing and nongrowing cells in response to antibiotics (**B**, top).

The list of author affiliations is available in the full article online.
*Corresponding author. E-mail: hwa@ucsd.edu

The Innate Growth Bistability and Fitness Landscapes of Antibiotic-Resistant Bacteria

J. Barrett Deris,[1,2]* Minsu Kim,[1]*† Zhongge Zhang,[3] Hiroyuki Okano,[1] Rutger Hermsen,[1,2]‡ Alexander Groisman,[1] Terence Hwa[1,2,3]§

To predict the emergence of antibiotic resistance, quantitative relations must be established between the fitness of drug-resistant organisms and the molecular mechanisms conferring resistance. These relations are often unknown and may depend on the state of bacterial growth. To bridge this gap, we have investigated *Escherichia coli* strains expressing resistance to translation-inhibiting antibiotics. We show that resistance expression and drug inhibition are linked in a positive feedback loop arising from an innate, global effect of drug-inhibited growth on gene expression. A quantitative model of bacterial growth based on this innate feedback accurately predicts the rich phenomena observed: a plateau-shaped fitness landscape, with an abrupt drop in the growth rates of cultures at a threshold drug concentration, and the coexistence of growing and nongrowing populations, that is, growth bistability, below the threshold.

The appearance of bacterial strains with broad antibiotic resistance is becoming an alarming global health concern. The rapidity with which drug resistance has emerged over the past 30 years, for both natural and synthetic antibiotics, exposes a glaring lack of understanding of drug-bacteria interaction and its evolution (*1*, *2*). Although thousands of genetic adaptations that enable drug resistance have been identified, this knowledge has not yet revealed how and when these adaptations will arise, that is, the underlying principles that determine the evolutionary pathways to drug resistance (*3*–*5*).

Although the success of a particular drug-resistant strain might depend on many factors, one of the most basic factors to consider is the nature of bacterial growth during antibiotic treatment. This is especially critical for resistance mechanisms evolved de novo, during early stages of evolution when drug resistance emerges in incremental steps (*3*, *6*, *7*). It is desirable to characterize the interaction between drug and drug resistance in exponentially growing cells because, during an infection, the number of bacteria can increase exponentially for many days (*8*, *9*); indeed, even as the host's immune response reduces the overall number of bacteria, individual bacteria that have yet to be killed are still estimated to grow at typical in vitro rates, doubling up to once or twice per hour for some pathogens (*10*, *11*). However, elucidating this interaction in growing cells is challenging because the expression of drug resistance genes, like the expression of any other gene, is often intimately coupled to the growth status of the bacteria (*12*–*18*).

In particular, translation-inhibiting antibiotics have been shown to reduce the expression of both regulated and constitutively expressed genes because of growth-mediated global effects (*16*, *17*). If one of these gene products provides some degree of antibiotic resistance, then growth inhibition can reduce expression of resistance; the diminished resistance can in turn allow the drug to further inhibit growth in a positive feedback loop (fig. S1), driving the cell into a stable nongrowing state after a transient slowdown in cell growth. Frequently, gene regulatory systems with positive feedback exhibit a switchlike behavior when, for example, intrinsic fluctuations in gene expression exceed some threshold (*19*, *20*). This is often accompanied by bifurcation of a genetically homogeneous culture into two subpopulations with distinct phenotypes, which is called bistability (*19*, *20*). In the context of antibiotic resistance, this would be manifested as a "growth bistability," that is, growing and nongrowing cells coexisting in a homogeneous environment.

[1]Department of Physics, University of California at San Diego, La Jolla, CA 92093–0374, USA. [2]Center for Theoretical Biological Physics, University of California at San Diego, La Jolla, CA 92093–0374, USA. [3]Section of Molecular Biology, Division of Biological Sciences, University of California at San Diego, La Jolla, CA 92093, USA.

*These authors contributed equally to this work.
†Present address: Department of Physics, Emory University, Atlanta, GA 30322, USA.
‡Present address: Theoretical Biology and Bioinformatics Group, Department of Biology, Faculty of Science, Utrecht University, Padualaan 8, 3584 CH Utrecht, Netherlands.
§Corresponding author. E-mail: hwa@ucsd.edu

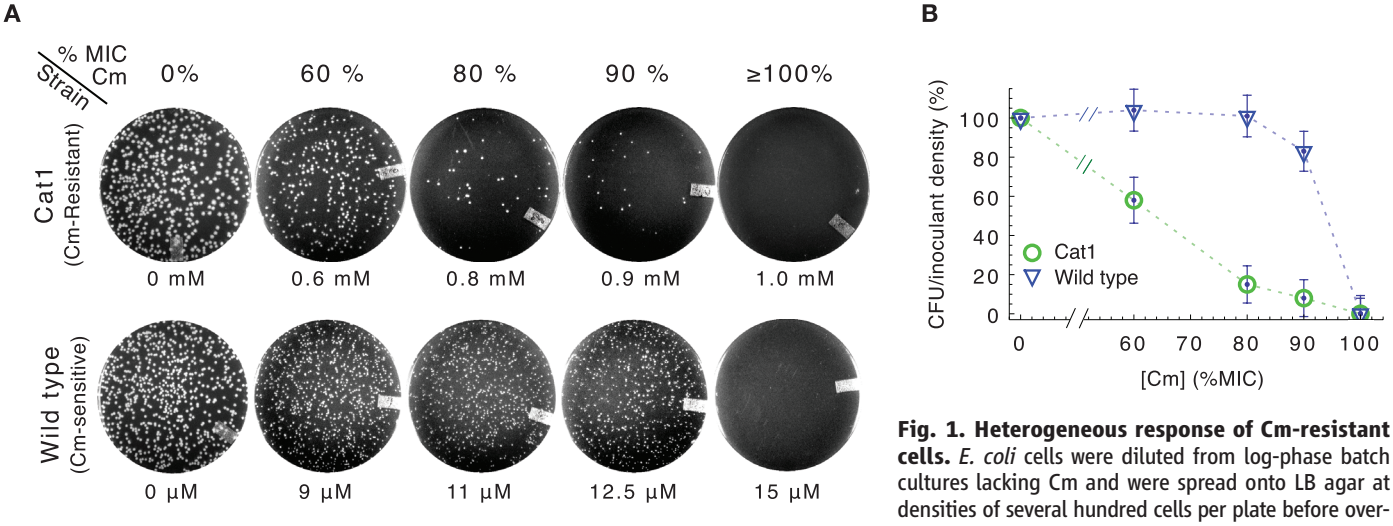

Fig. 1. Heterogeneous response of Cm-resistant cells. *E. coli* cells were diluted from log-phase batch cultures lacking Cm and were spread onto LB agar at densities of several hundred cells per plate before overnight incubation at 37°C. (**A**) Typical plate images of Cm-resistant Cat1 (top row) and Cm-sensitive wild-type (bottom row) cells, with Cm concentration indicated below each plate and also given above as approximate fraction of the empirically determined MIC_{plate} for each strain (figs. S2A and S3A). (**B**) Percentage of viable cells grown on Cm-LB plates, CAT-expressing cells (Cat1, green), and wild-type cells (EQ4, blue). Error bars estimate SD of CFU, assuming Poisson-distributed colony appearance.

To characterize the nature of drug–drug resistance interactions and the possible occurrence of growth bistability, we studied the growth of various *Escherichia coli* strains constitutively expressing varying degrees of resistance to translation-inhibiting antibiotics. Our observations at both population and single-cell levels show that drug-resistant strains exhibit many signatures of growth bistability in response to antibiotics, contradicting the naïve expectation that constitutive expression of drug resistance in a population of cells will provide uniform protection against the drug. As will be shown, a heterogeneous effect of antibiotics on genetically identical cells challenges common notions and measures of drug efficacy and resistance and exposes both limitations and opportunities for treatment strategies.

We proceed to develop a simple mathematical model that effectively captures the origins of the observed behaviors and accurately predicts the growth rates of antibiotic-resistant cells in the presence of drugs without invoking any ad hoc fitting parameters. These results reveal a plateau-like fitness landscape that describes an abrupt transition between growth and growth inhibition for strains expressing a broad range of drug resistance subjected to a broad range of drug concentrations. Quantitative knowledge of the fitness landscape is vital for understanding and predicting the evolvability of drug resistance, for example, the acquisition of antibiotic resistance in a stepwise manner.

Results

Heterogeneous Responses to Antibiotics

Antibiotic susceptibility is typically assayed by counting the colonies formed after bacteria are spread onto agar plates containing various concentrations of antibiotics (*21*). If these cells exhibit growth bistability, then only the growing fraction of the inoculant cells will form colonies. To test for this heterogeneous response, we characterized the fraction of colonies formed by various strains of *E. coli* growing on agar in the presence of chloramphenicol (Cm), one of the oldest and most-studied translation-inhibiting antibiotics (*22*). We studied strains that express the Cm-resistance enzyme chloramphenicol acetyltransferase (CAT), which modifies and deactivates Cm according to well-characterized biochemistry (*23*). CAT enzymes are expressed constitutively in our strains, just as they (and many other drug-resistance enzymes and pumps) are often found in the wild (*24*–*27*).

Overnight incubation of CAT-expressing strains on Cm agar plates revealed signs of population-level heterogeneity. For one such strain, Cat1 (table S1), the number of colony-forming units (CFU) decreased gradually on plates with increasing Cm concentrations [Fig. 1A (top) and fig. S2B]. Thus, only a fraction of the plated cells formed visible colonies (Fig. 1B, circles), even at concentrations well below the empirical minimal inhibitory concentration at which colony formation is completely inhibited (MIC_{plate}, fig. S2A). It is unlikely that heterogeneity arose from spontaneous mutation because repeating the experiment using a single colony isolated at 90% MIC_{plate} produced qualitatively similar results (with CFU decreasing at intermediate drug levels, fig. S2, C and D). In contrast, the CFU count of CAT-less wild-type cells (strain EQ4) remained high until complete inhibition at MIC_{plate} [Fig. 1A (bottom) and fig. S3], indicating that the vast majority of plated cells grew up to the MIC (Fig. 1B, triangles).

Direct Observation of Growth Bistability by Microscopy

To verify the coexistence of growing and nongrowing cells directly, we used a microfluidic device in which the growth of individual (immotile) cells could be tracked with time-lapse microscopy for extended periods (*28*) as they grew in the presence of Cm. The device provides a steady supply of fresh medium to many growth chambers, whose heights are adjusted to be slightly larger than the width of a single bacterium (~1 μm), allowing cells to grow for up to about nine generations into monolayer colonies in each chamber (fig. S4). Immotile CAT-expressing cells (Cat1m) growing exponentially in Cm-free batch culture were transferred to the microfluidic device and were allowed to continue growing exponentially for several generations before switching to growth medium with Cm (see Materials and Methods). With 0.9 mM Cm (90% of MIC_{plate}) in the medium, 70% of the cells stopped growing; nongrowing and growing cells were often observed side by side in the same chamber (Fig. 2A and movie S1). Eventually, it became impossible to track these nongrowing cells that were adjacent to growing populations because of overcrowding. By tracking some nongrowing cells that were far away from growing populations, we observed that this growth bimodality persisted for the duration of observation (up to 24 hours) because cells rarely switched between the growing and nongrowing states at 0.9 mM Cm (less than 1%).

One possible explanation for the sustained presence of nongrowing cells is that these cells did not have the *cat* gene at the beginning of the experiment. To see whether the heterogeneous response observed was due to (unintended) heterogeneity in genotype (for example, contamination), we reduced Cm concentration in the chambers from 0.9 to 0.1 mM, a concentration well above the MIC of Cm-sensitive cells (fig. S3). Many nongrowing cells began growing again, sometimes within ~5 hours of the Cm downshift (Fig. 2B and movie S2), indicating that previously nongrowing cells carried the *cat* gene and were viable [although Cm can be bactericidal at high concentrations (*29*)]. Thus, the population of cells in the nongrowing state was stable at 0.9 mM Cm (at least over the 24-hour period tested) but unstable at 0.1 mM Cm, suggesting that growth bistability might only occur at higher Cm concentrations.

Repeating this characterization for Cat1m cells at different Cm concentrations revealed that the fraction of cells that continued to grow decreased gradually with increasing concentration of the Cm added (Fig. 2C, height of colored bars), qualitatively consistent with the Cm-plating results for Cat1 cells (Fig. 1B). At concentrations up to 0.9 mM Cm, the growing populations grew exponentially, with their growth rate decreasing only moderately (by up to ~50%) with increasing Cm concentrations [Fig. 2, C (hue) and D (green symbols)]. Growing populations disappeared completely for [Cm] ≥ 1.0 mM, marking an abrupt drop in growth between 0.9 and 1.0 mM Cm (green and black symbols in Fig. 2D). This behavior contrasts with that observed for the Cm-sensitive wild type, in which nearly all cells continued growing over the entire range of subinhibitory Cm concentrations tested in the microfluidic device (Fig. 2E). This result is consistent with the response of wild-type cells to Cm on agar plates (Fig. 1), indicating that growth in subinhibitory concentrations of Cm per se does not necessarily generate growth bistability.

The Abrupt Onset of Growth Bistability

Infrequently, we also observed nongrowing wild-type cells in microfluidic experiments, although their occurrence was not correlated with Cm concentration (r_s ~0.1). This is not surprising because exponentially growing populations of wild-type cells are known to maintain a small fraction of nongrowing cells in the phenomenon called "persistence" (*30*). In the natural course of exponential growth, wild-type cells have been shown to enter into a dormant persister state stochastically at a low rate, resulting in the appearance of one dormant cell in every ~10^3 to 10^4 growing cells (*31*–*33*). It is possible that the growth bistability observed for the CAT-expressing cells in low Cm concentrations is due to such naturally occurring persistence (referred to below as "natural persistence"). This question cannot be resolved by our current microfluidic experiments, which, at a throughput of ~10^3 cells, can barely detect natural persistence. We therefore sought a more sensitive method to quantify the conditions that produce growth bistability.

To enhance the sensitivity for detecting nongrowing cells and to probe the population-level behavior of Cat1 cells in batch cultures, we adapted an ampicillin (Amp)–based enrichment assay (*34*) that isolated nongrowing cells from Cm-containing cultures. This enrichment assay (fig. S5) took advantage of the fact that Amp only kills growing cells (*35*), thereby enriching cultures for potentially dormant cells to later be revived in the absence of antibiotics. With the microfluidic device, we verified visually that the cells that stopped growing because of Cm-induced growth bistability could survive Amp treatment, and were viable when antibiotics were removed (fig. S6).

In batch culture enrichment, Cat1 cells that failed to grow in the presence of Cm later appeared as colonies on antibiotic-free agar plates (fig. S7A). Consistent with the results in the microfluidic chamber (Fig. 2C), the fraction of

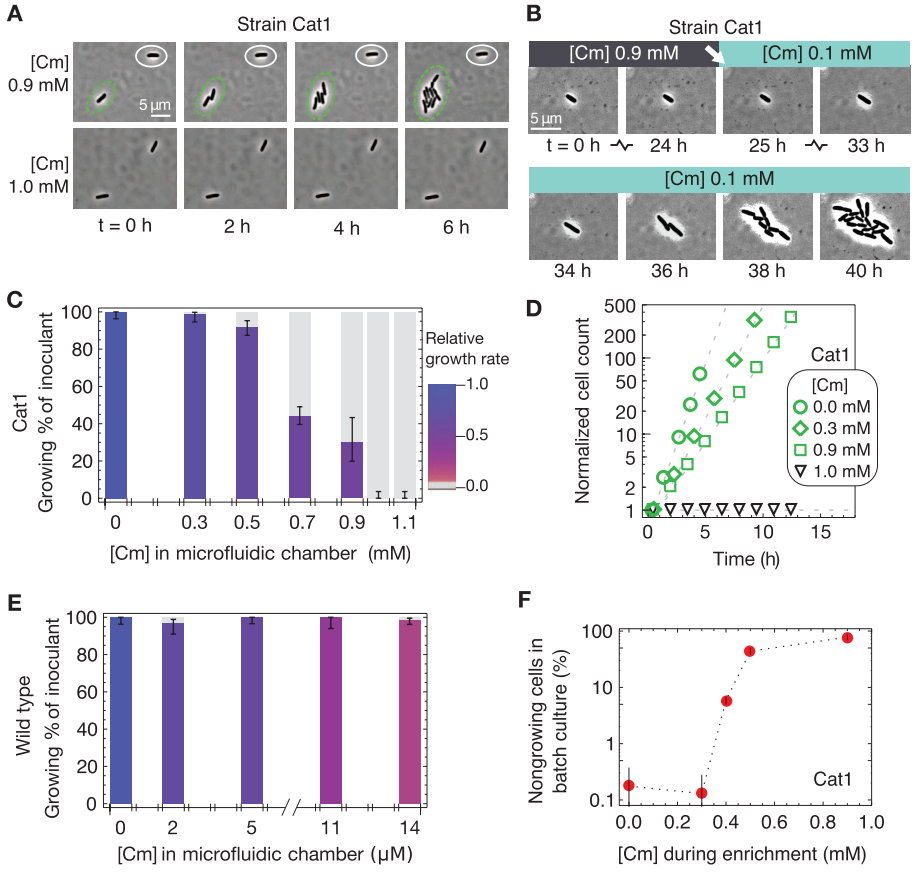

Fig. 2. Drug-induced growth bistability. (**A**) Upon increasing Cm concentration from 0 to 0.9 mM in microfluidic chambers (fig. S4), genetically identical Cat1m cells growing exponentially in glucose minimal medium either continued growing (circled in green) or were growth-arrested (circled in white); see movie S1. None of the Cat1m cells grew after adding Cm to 1.0 mM. (**B**) A typical example of the cells that remained dormant throughout the 24 hours during which microfluidic chambers contained 0.9 mM Cm; growth resumed ~8 hours after Cm was reduced to 0.1 mM, which is still well above the MIC of wild-type cells (see movie S2). (**C**) Height of colored bars gives the percentage of Cat1m cells to continue exponential growth in microfluidic chambers upon adding the indicated concentration of Cm; error bars give 95% confidence interval, assuming a binomial distribution. Bar color indicates growth rates of growing cells, with the relative growth rate given by the scale bar on the right. (**D**) Growth curves at different Cm concentrations, given by the size of growing colonies (*y* axis) in the microfluidic device. The deduced growth rates dropped abruptly from 0.35 hour^{-1} (green squares) at 0.9 mM Cm to zero at 1.0 mM Cm (black triangles). (**E**) As in (C), but for immotile wild-type cells (EQ4m) that showed no significant correlation between growth rate and fraction of growing cells (r_s ~0.1). (**F**) Fraction of Cat1 cells remaining after the batch culture Amp-Cm enrichment assay (fig. S5). The results (fig. S7) reveal significant fractions of nongrowing cells well above the basal level of natural persisters (~10^{-3}), for [Cm] ≥ 0.4 mM until the MIC of 1.0 mM, above which no cells grew. Error bars estimate SD of CFU, assuming Poisson-distributed colony appearance.

nongrowing cells identified by the enrichment assay at 0.3 mM Cm and below was small (≤10^{-3}, Fig. 2F), comparable to the frequencies characterized for natural persistence under similar conditions (*31*, *32*). However, the frequency of cells in the nongrowing state increased substantially at [Cm] ≥ 0.4 mM (Fig. 2F and fig. S7A). We define the minimal coexistence concentration (MCC) as the lowest antibiotic concentration above which coexistence between growing and nongrowing cells appears at frequencies significantly above natural persistence; MCC ≈ 0.35 mM for the strain Cat1. Thus, growth bistability turns large fractions of Cm-resistant cells into Cm-sensitive cells at Cm concentrations between MCC and MIC. In contrast, enriching Cm-sensitive wild-type cells in subinhibitory Cm concentrations reveals that most cells grow; >99% remain sensitive to Amp for all sub-MIC Cm concentrations (fig. S7B), which is consistent with previous findings that cells should only be protected from Amp if Cm completely inhibits growth (*35*–*37*).

Growth-Mediated Feedback and Generic Growth Bistability

If growth bistability exhibited by Cat1 cells was indeed a result of generic growth-mediated feedback, then it should appear generally, not just idiosyncratically for Cm and the specific action of the Cm-modifying enzyme CAT. Toward this end, we tested the growth of a strain (Ta1) constitutively expressing the tetracycline efflux pump TetA (*38*, *39*) in microfluidic chambers with medium containing various concentrations of the drug tetracycline (Tc). As with the growth of strain Cat1 in Cm, Ta1 exhibited coexistence of growing and nongrowing cells for a range of sub-MIC concentrations of Tc and an abrupt drop in its relative growth rate at the MIC (from ~60% of the uninhibited rate to no growth, fig. S8A). In contrast to Tc-resistant cells, none of the wild-type cells stopped growing when exposed to sub-MIC Tc concentrations, even when Tc reduced growth rate by 85% (fig. S8C). These results were similar to those for Cat1 cells in Cm, supporting the hypothesis that growth bistability occurs generically, independent of the mode of drug resistance, as is predicted by growth-mediated feedback (fig. S1).

Quantitative Model for Antibiotic-Resistant Growth

To determine whether growth-mediated feedback could quantitatively account for the occurrence of growth bistability (Figs. 1 and 2), we developed a simple mathematical model to predict the effect of a drug on the growth of cells constitutively expressing drug resistance. We focus here on the Cm-CAT system, whose biochemistry is quantitatively characterized (*23*); (*40*) contains a more general treatment with respect to other antibiotics and resistance mechanisms. The model contains three components, as summarized in Fig. 3A, and can quantitatively predict the dependence of the steady-state growth rate on the Cm concentration of the medium: (i) At steady state, the relation between the internal and external Cm concentration ($[Cm]_{int}$ and $[Cm]_{ext}$, respectively) can be obtained by balancing the rate of Cm influx with the rate of Cm clearance by CAT. (ii) The concentration and, hence, activity of constitutively expressed CAT proteins depends linearly on a cell's growth rate in response to applied Cm as a result of global growth-dependent effects. (iii) The cell's doubling time depends linearly on $[Cm]_{int}$ through the known effect of Cm on translation. Below, we elaborate on each component in some detail.

Balance of Drug Influx and Clearance

We assume that Cm influx is passive (*41*), as described by Eq. 1 in Fig. 3B, with a permeability κ (table S2). The Cm-CAT interaction is described by Michaelis-Menten kinetics (*23*) parameterized by K_m and V_{max} (Eq. 2 in Fig. 3B). Solving Eqs. 1 and 2 yields an approximate threshold-linear dependence of $[Cm]_{int}$ on $[Cm]_{ext}$ (red line in Fig. 3B). According to this nonlinear relation, $[Cm]_{int}$ is kept relatively low for external concentrations up to ~V_{max}/κ, the threshold concentration above which Cm influx reaches the maximum capacity of Cm clearance by CAT. Note that this buffering

effect does not require any molecular cooperativity (*40*).

Growth Rate–Dependent Expression of Constitutive (Unregulated) Genes

Figure 3C shows that, under translation-limited growth, the expression levels (that is, protein concentrations) of unregulated genes decrease linearly with decreasing growth rate λ (*16*, *42*). This trend contradicts the commonly held expectation that protein concentration should decrease with increasing growth rates, owing to a growth-mediated dilution effect. Instead, the proportionality between expression level and growth rate follows from bacterial growth laws (*16*) and can be understood as a generic consequence of the up-regulation of ribosome synthesis upon translational inhibition, at the expense of the expression of nonribosomal genes (fig. S9). The behavior is shown for translation-inhibited growth in Fig. 3C, with CAT activity (V_{max}) of cells constitutively expressing CAT (open green circles) and LacZ activity of cells constitutively expressing LacZ (open black symbols). This result is described by Eq. 3 in Fig. 3C, expressed relative to the CAT activity and growth rate in cells not exposed to drugs (denoted by V_0 and λ_0, respectively). We note that some drug resistance genes are not usually expressed constitutively, but require induction by the target antibiotic (*25*–*27*). However, regulated gene expression is still subject to growth-mediated feedback (*17*, *43*) and may suffer substantial reduction upon increasing the drug concentration. This has been observed for the native Tc-inducible promoter that controls Tc resistance, for growth under sublethal doses of Tc (fig. S10).

Effect of Translation Inhibition on Cell Growth

For exponentially growing cells subjected to subinhibitory doses of Cm, the relative doubling time (λ_0/λ) is expected to increase linearly with internal drug concentration $[Cm]_{int}$; see Eq. 4 in Fig. 3D. This relation is a consequence of the characterized effects of Cm on translation (*22*) together with bacterial growth laws, which dictate that the cell's growth rate depends linearly on the translation rate of the ribosomes (fig. S9) (*16*, *44*). Growth data in Fig. 3D verify this quantitatively for wild-type cells. The lone parameter in this relation, the half-inhibition concentration I_{50}, is governed by the Cm-ribosome affinity (eq. S6), and its empirical value is well accounted for by the known biochemistry (*22*) (table S2).

Comparing Model Predictions to Experimental Observations

The Value of the MIC

The model based on the above three components contains three parameters: K_m, I_{50}, and V_0/κ. The first two are known or measured in this work (table S2), whereas the last one, reflecting the basal CAT activity level (V_0), is construct-specific. The model predicts a precipitous drop of growth rate across a threshold Cm concentration, which we identify as the theoretical MIC, whose value depends linearly on V_0/κ as given by eq. S28. Empirically, an abrupt drop in growth rate is indeed apparent in the batch culture (fig. S11), yielding an MIC value (0.9 to 1.0 mM) that agrees well with those determined in microfluidics and plate assays. Comparing this empirical MIC value with the predicted dependence of MIC on V_0/κ (eq. S28) fixes this lone unknown parameter to a value compatible with an independent estimate, on the basis of the measured CAT activity V_0 and indirect estimates of the permeability value κ (table S2).

Dependence on Drug Concentration

With V_0/κ fixed, the model predicts Cm-dependent growth rates for this strain without any additional parameters (black lines, Fig. 4A). The upper branch of the prediction is in quantitative agreement with the growth rates of Cat1 measured in batch culture [Fig. 4A (solid circles) and fig. S11]. Additionally, when we challenged Tc-resistant strain Ta1 with either Tc or the Tc analog minocycline (Mn) (*39*), the observed growth rates also agreed quantitatively with the upper branch of the respective model predictions (fig. S12). Note also that in the absence of drug resistance or efflux, Eq. 4 predicts a smoothly decreasing growth rate with increasing drug concentration, which we observed for the growth of wild-type cells over a broad range of concentrations (figs. S8C and S12C).

The model also predicts a lower branch with very low growth rates and a range of Cm concentrations below MIC where the upper and lower branches coexist (Fig. 4A, shaded area). We identify the lower edge of this band as the theoretical MCC because a uniformly growing population is predicted for Cm concentrations below this value. Indeed, the occurrence of nongrowing cells for strain Cat1 (Fig. 4A, open diamonds) coincided with the shaded area. Likewise for strain Ta1, respective microfluidic and Amp enrichment experi-

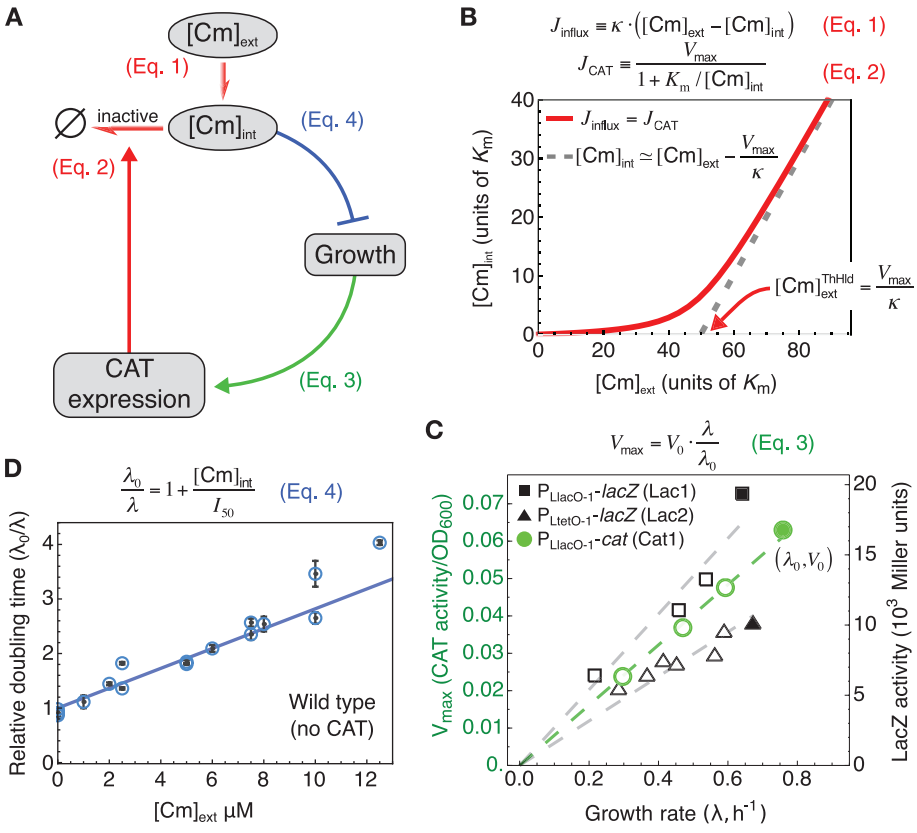

Fig. 3. Growth-mediated feedback. (**A**) Components of interactions defining the feedback model. Each link describes a relation substantiated in (B) to (D) (clockwise). (**B**) The relationship between the internal and external Cm concentrations ($[Cm]_{int}$ and $[Cm]_{ext}$, respectively), described by the red line, is obtained by balancing the passive influx of Cm into the cell (J_{influx}, Eq. 1) with the rate of Cm modification by CAT (J_{CAT}, Eq. 2). This nonlinear relation is characterized by an approximate threshold-linear form, with a "threshold" Cm concentration, $[Cm]_{ext}^{threshold}$ (red arrow), below which $[Cm]_{int}$ is kept low as the capacity for clearance by CAT well exceeds the Cm influx (eq. S12). For $[Cm]_{ext} > [Cm]_{ext}^{threshold}$, CAT is saturated and $J_{influx} \approx V_{max}$ (dashed gray line). (**C**) The expression levels of constitutively expressed CAT (green) and LacZ (black) reporters [reported here in units of activity per OD (*42*)] are proportional to the growth rate with subinhibitory doses of Tc and Cm, respectively. (**D**) The doubling time (blue circles) of wild-type (EQ4) cells grown in minimal medium with various concentrations of Cm increases linearly with [Cm] (Eq. 4). I_{50} (dashed vertical line) gives the Cm concentration at which cell growth is reduced by 50%. Here, $[Cm]_{int} \approx [Cm]_{ext}$ because of the absence of endogenous Cm efflux for wild-type cells in minimal medium (*41*) (see also eq. S9). Each point represents a single experiment; error bars of the doubling times are SEs of inverse slope in linear regression of $\log(OD_{600})$ versus time.

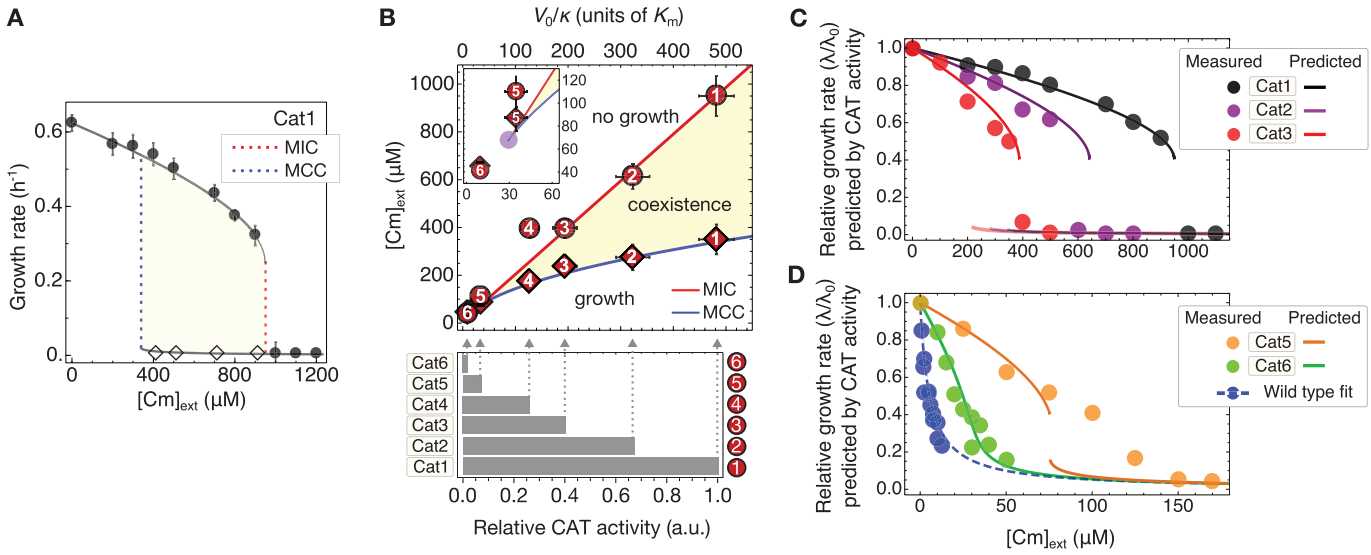

Fig. 4. Growth rate predictions and phase diagram. (**A**) The growth rate of Cat1 strain in minimal medium batch culture with varying Cm concentrations (solid circles) agrees quantitatively with the prediction of the growth feedback model (line) on the basis of the measured MIC (dashed red line). Error bars, SD; $n \geq 3$. Dashed blue line is the theoretical MCC. Diamonds indicate drug levels at which enrichment experiments identified significant numbers of nongrowing cells (fig. S7). (**B**) The MCC (blue line) and MIC (red line) predicted by the growth feedback model for strains with different degrees of basal CAT expression (V_0) define a phase diagram, with the coexistence of growing and nongrowing populations between the MCC and MIC (beige). MIC (circles, fig. S14) and MCC (diamonds, fig. S15) are measured for strains differing only in their levels of constitutive CAT expression (quantified by the relative CAT activity in the absence of Cm, given by the bar graph below). Error bars, SD; $n \geq 2$. (**C** and **D**) Measured and predicted growth rates (circles and lines of like colors) in minimal medium with varying Cm concentrations for strains of known relative CAT activities; the wild type is shown in blue for reference. Predictions were obtained by solving eq. S28 for V_0/κ, using the measured MIC for strain Cat1 and the measured relative CAT activity between the different strains [bottom of (B)], without any parameter fitting.

ments with Tc (fig. S8) and Mn (fig. S13) revealed nongrowing cells within the theoretical coexistence region (lower branches in fig. S12).

Dependence on CAT Expression: Phase Diagram

The growth-mediated feedback model makes quantitative predictions on how the MIC and MCC depend on the basal CAT expression of the strain (V_0/κ), as shown in the phase diagram of Fig. 4B. The MIC (red line) is predicted to increase linearly with V_0/κ, whereas the MCC (blue line) is predicted to increase as $\sqrt{V_0/\kappa}$ (eqs. S28 and S39, respectively). These two lines define a wedge in the parameter space of $[Cm]_{ext}$ and $\sqrt{V_0/\kappa}$, terminating at a bifurcation point (purple point in inset), below which a uniformly growing population is predicted (see eq. S24). We tested these predictions by using five additional strains (Cat2 through Cat6; tables S1 and S3) designed to provide reduced degrees of constitutive CAT expression; see quantitation of V_0 for each strain at bottom of Fig. 4B. Assuming that the permeability κ does not differ significantly across these strains, the measured CAT activities give V_0/κ for all strains (relative to that of Cat1), as shown by the gray arrows in Fig. 4B. Figure 4B also displays the batch culture MIC (comparable to MIC_{plate} values, fig. S14) and MCC values (fig. S15) obtained for these strains as numbered circles and diamonds, respectively. The model predictions (lines) capture these observations well except close to the bifurcation point (for example, in strain Cat5, inset), without adjusting any parameters. Note that because the feedback model is based on steady-state relations (Eqs. 3 and 4), it is not expected to describe the kinetics of transition into the nongrowing state or its frequency of occurrence, both of which likely depend on complex stochastic processes. However, in all our experiments, we never observed growth bistability at drug concentrations below the predicted MCC.

The CAT activities (V_0/κ; Fig. 4B, bottom) can also be used to predict growth rate reductions (λ/λ_0) for these strains for concentrations below the MIC. The predictions are plotted together with the data (lines and circles of like colors) in Fig. 4, C and D. The predictive power of the model is rather remarkable because the lines are not fits to the data, but merely solutions to eqs. S15 and S5, using the measured values of V_0 as input. Comparable agreements are obtained using the empirical MIC value for each strain (fig. S16). In contrast, an identical model lacking growth-mediated feedback cannot account for the Cm dependence of the growth rates of these strains, particularly the abrupt drop in growth at MIC in strains Cat1 to Cat3 (fig. S17). Even incorporating stochasticity into this deterministic alternative model could not resolve this basic qualitative disagreement with our observations [see (*40*), section 2.5].

Fitness Landscapes

Figure 5A gives the full solution of the model for strains with a range of CAT activity (V_0/κ) in medium with varying Cm concentrations ($[Cm]_{ext}$). The colored lines reproduce the predicted growth rates of several strains from Fig. 4, C and D, and span a range of behaviors, from subcritical to bistable. Viewing this plot orthogonally, the white line illustrates growth rates in an environment of fixed Cm concentration for strains of different CAT activities. Whereas the CAT activity levels (V_0) are determined directly by molecular properties encoded by the genotype, for example, the promoter or ribosomal binding sequences (table S3) and the coding sequence of the *cat* gene, the white line describes a relation between the growth rate and the genotype, and may be regarded as a "fitness landscape." There is such a fitness landscape for each environmental Cm concentration. For $[Cm]_{ext} > [Cm]_{ext}^{crit}$, these fitness landscapes are plateau-shaped, characterized by a threshold level of CAT activity (survival resistance threshold, V_{SRT}) across which the growth of the culture changes abruptly (Fig. 5B, diagonal dashed line).

A recent theoretical analysis (*45*) characterizes how bacteria can evolve through plateau-shaped fitness landscapes with drug-dependent survival thresholds and demonstrates how landscape structure can determine the rate at which antibiotic resistance emerges in environments that precipitate rapid adaptation (*45*–*47*); see illustration in Fig. 5B. Specifically, in environments containing a spatial gradient of drug concentrations, the plateau-shaped landscape ensures that a large population of cells is always near an uninhabited niche of higher drug concentration (due to the respectively high and low growth rates on either side of the threshold). Therefore, mutants in this population expand into regions of higher drug

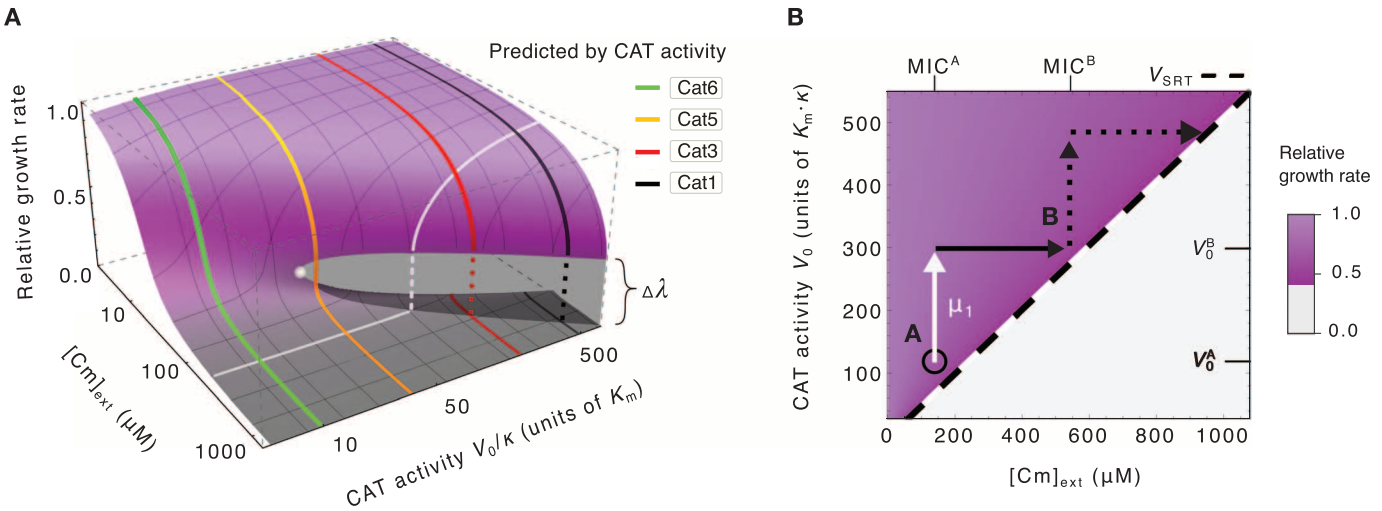

Fig. 5. Fitness landscapes of drug resistance. (**A**) Predicted growth rates (height of surface) for arbitrary CAT activity and Cm levels (V_0 and $[Cm]_{ext}$, respectively): High (purple surface) and low growth rates (gray surface) overlap in the region of coexistence (growth bistability) that terminates at the bifurcation point (filled white circle). Predictions from Fig. 4, C and D, are reproduced (colored lines). The orthogonal white line illustrates the expected effect of changing CAT activity at a fixed Cm concentration; it can be viewed as a plateau-shaped fitness landscape. (**B**) The survival resistance threshold required for growth, V_{SRT}, is predicted to vary linearly with the drug concentration (diagonal black dashed line). For a population initially at point A (black circle) in the phase diagram, that is, with resistance activity V_0^A and surviving in niches with $[Cm]_{ext} < MIC^A$, a mutation (μ_1, white arrow) that increases the resistance activity level to V_0^B can allow the bacteria to "expand its range" (*45*) and proliferate into all niches with $MIC^A \leq [Cm]_{ext} \leq MIC^B$ without competition (solid black arrow). Additional mutations, for example, upstream of the gene at the ribosomal binding sequence (see table S3), or gene amplification events (*69*) provide a simple pathway for sequential expansions into increasingly harsh environments (*45*, *70*).

concentration without competition, and adaptation like this can continue in a ratchetlike fashion to allow the population to survive in increasingly higher concentrations of antibiotics.

Discussion

The drugs investigated in this study (Cm, Tc, and Mn) are infrequently prescribed today. Because of this, they are among only a handful of antibiotics that remain effective against "pan-resistant" bacteria, that is, those resistant to all other standard drugs and polymyxins, and have been advocated as a last line of defense (*48*, *49*). Therefore, understanding the effect of these drugs on drug resistance expression is critical. More broadly, many other antibiotics also affect gene expression in a variety of bacteria and fungi (*13*, *50*, *51*), raising general questions about the effect of drug–drug resistance interaction on cell growth, the consequences of this interaction on the efficacy of treatment programs, and the long-term evolvability of drug resistance.

We have shown here that for the class of translation-inhibiting antibiotics, the fitness of resistance-expressing bacteria exposed to antibiotics can be quantitatively predicted with a few empirical parameters that are readily determined by the physiological characteristics of the cells. Our minimal model is based on the physiology of drug-cell interactions and the biochemistry of drug resistance. Although it neglects many details, for example, the fitness cost of expressing resistance that may matter when small differences in fitness determine the emergence of resistance (*52*, *53*), this minimal approach already captures the generic existence of a plateau-shaped fitness landscape that can facilitate emerging drug-resistant mutants to invade new territories without competition (*45*). These plateau-shaped fitness landscapes accompany the phenomenon of growth bistability, which arises from positive feedback. As demonstrated here, these positive feedback effects do not require special regulatory mechanisms or any molecular cooperativity and are not limited to a specific enzymatic mechanism of drug resistance. Furthermore, these effects cannot be understood by merely analyzing some local genetic circuits but are instead derived from the global coordination of gene expression during growth inhibition (*16*). Therefore, we expect the growth bistability and the accompanying plateau-shaped fitness landscape to be robust features innate to drug-resistant bacteria.

Growth bistability in drug response has previously been theorized to occur for bacteria lacking drug resistance and for antibiotics with low membrane permeability (*54*). These considerations are not applicable to the systems we study here, because wild-type cells grew homogeneously in the presence of antibiotics tested, and only cells expressing drug resistance exhibited growth bistability when cultured in the presence of antibiotics. The observed growth bistability is also unlikely to arise from a recently described inoculum effect (*55*), in which two separate cultures with identical concentration of certain drugs may exhibit distinct growth rates depending on the culture inoculant density: First, the bacteriostatic drugs investigated here (Cm and Tc) have been shown not to exhibit the inoculum effect (*55*, *56*). Second, the inoculum effect concerns the differences between separate cultures, whereas we observed coexistence of growing and nongrowing subpopulations in a single homogeneous culture.

We also considered the relationship between the drug-induced growth bistability studied here and the phenotypic bistability implicated in natural persistence, identified as the source of many long-term, refractory bacterial infections (*19*, *57*, *58*). These are, first of all, clearly distinct phenomena that nevertheless can be easily be mistaken for one another: The effect we studied is an innate response to drug for cells carrying drug resistance, whereas natural persistence refers to spontaneous entry into the nongrowing state (which can occur in the absence of drugs) for drug-sensitive strains. Also, the frequency of nongrowing cells is typically very low (~0.1%) in natural persistence, but it can be macroscopic (even greater than 80%) for the drug-induced effect. Finally, a cell achieves natural persistence by producing toxin proteins to inhibit its own growth (*33*, *58*), whereas the effect studied here is an obligatory response to applied drugs, rooted deeply in the organization of bacterial growth control (*16*).

However, there also exist important parallels between these two phenomena that cannot be overlooked and may be exploited to understand natural persistence: Researchers have devoted many efforts and resources to understanding the mechanisms underlying bistability in natural persistence, whereas here we show that bistability can arise without complex regulation when gene expression is coupled to the state of cell growth. A similar general strategy may also underlie natural persistence, with cell growth inhibited by a

toxic endogenous gene product whose expression would likely be affected by global growth-dependent effects (*57*–*59*). The precise effects of growth inhibition on gene expression will depend on the specific mode of growth limitations imposed upon cellular metabolism by the various toxin systems (*60*). Characterizing these feedback effects, in the manner we have done here for antibiotic resistance, may yield critical clues needed to formulate a quantitative, physiological understanding of natural persistence.

The fact that drugs can induce growth bistability, that is, antibiotics can have a wildly heterogeneous effect on genetically identical cells in a homogeneous environment, calls into question the current methods of characterizing drug efficacies, which are often performed in bulk growth conditions (*21*). It provides a new perspective on basic notions of drug resistance, including the MIC, which begs for a more careful empirical definition to avoid vast inconsistencies across laboratories (*61*, *62*). Remarkably, large fractions of bacterial cells can remain vulnerable to an antibiotic (that is, stop growing) even though they carry genes providing resistance to it; understanding the mechanisms that force cells into the nongrowing state could enable the development of new treatment strategies against drug-resistant bacteria. On the other hand, heterogeneous effects may require a more careful reexamination of the effectiveness of combinatorial drug treatment (*43*, *63*) because strains resistant to one drug may produce macroscopic fractions of growing and nongrowing cells that respond very differently to a second drug, which may affect the evolution of drug resistance (*63*). The success of the phenomenological model presented here for the class of translation-inhibiting antibiotics gives the hope that predictive models may be similarly developed for other types of drug action, including combinations of drugs, to facilitate the formulation of strategies that limit the efficacy and evolvability of drug resistance.

Materials and Methods

Culture and Cell Growth

Media and Chemicals

Unless noted elsewhere, minimal medium refers to a mixture of 0.4% (w/v) glucose, 20 mM NH_4Cl, and "N$^-$C$^-$" buffer (*64*) consisting of 1.0 g of K_2SO_4, 17.7 g of K_2HPO_4•$3H_2O$, 4.7 g of KH_2PO_4, 0.1 g of $MgSO_4$•$7H_2O$, and NaCl (2.0 g/liter), with 6 mM sodium acetate when indicated. Chloramphenicol (Sigma C0378) stock solutions contained Cm at a concentration of either 2 or 25 mg/ml in 70% isopropanol stock solution. Tetracycline hydrochloride (Sigma T4062) stock solutions contained Tc•HCl at a concentration of either 0.1 or 25 mg/ml in deionized H_2O; minocycline hydrochloride (Sigma M9511) stock solution contained 10 mM Mn•HCl. These stock solutions were stored at −20°C in the dark and used for preparation of media with various concentrations of antibiotics. Antibiotics were added to the media at the time of experiment as described below, and for Cm, stock concentration was chosen such that the volume added would not exceed 1.5% of total medium volume.

LB agar plates containing Cm were prepared on the day of experiments as follows: After freshly mixed LB agar was autoclaved, 100-ml aliquots were poured into 250-ml Erlenmeyer flasks and cooled to about 50°C. A volume of Cm solution was then pipetted from an appropriate stock into the liquid agar (to achieve the desired concentration), and the mixture was swirled both clockwise and counterclockwise for 10 s. We then poured about 25 ml of medium plus agar into each 100 mm × 15 mm petri dish (Fisherbrand).

Batch Culture Growth

All batch cultures grew at 37°C in a water bath shaker at 250 rpm (New Brunswick Scientific G76D) with a covered basin to protect photosensitive chemicals (for example, Tc) from degradation and to prevent heat bath from evaporating. Culture growth measurements were performed with unique seed cultures each day. Each 5 ml of seed culture grew to saturation in LB broth from a single colony on an LB plate. Seed cultures were diluted into 5-ml precultures containing minimal media and grown overnight without antibiotic. Except as noted below, experimental cultures were diluted from overnight precultures into 5 ml of minimal medium supplemented with appropriate antibiotics in 20-mm-diameter glass tubes. Experimental cultures were inoculated to an initial optical density (OD_{600}) ~0.01, as measured by a Thermo Scientific Genesys 20 spectrophotometer, with a Starna Cells quartz cuvette with a 10-mm light path. At intervals ranging from 40 min to 2 hours, we took 250-µl samples from growing cultures to measure OD_{600}. For growth in Tc or Mn, to control for thermolability or photosensitivity (*65*, *66*), we diluted growing cultures 10- to 20-fold into fresh identical media to verify that culture age did not affect growth rate over the course of our experiments.

Growth of Strains Expressing CAT in Cm

We followed the same procedure as described above, except we began the experiments with ~60-fold lower cell densities in bulk cultures to avoid significant degradation of Cm by CAT during the course of growth. Briefly, experimental cultures were diluted from overnight precultures into a larger volume of 10 ml of minimal medium supplemented with appropriate Cm and acetate in larger 25-mm-diameter glass tubes. From the larger experimental culture volume, we pipetted 1 ml of samples into a Starna Cells quartz cuvette with a 40-mm light path to record OD. Use of the cuvette with longer path length allowed us to observe cultures at fourfold lower densities using the same Genesys spectrophotometer as above. Experimental cultures were inoculated to a maximum initial density of OD_{600}^{4x} ~0.0007 determined by the larger cuvette (OD_{600} ~0.0002). In this manner, we were able to achieve steady exponential growth observable up to at least OD_{600}^{4x} ~0.1 with this cuvette (see green symbols in fig. S11).

Determination of Growth Rate and MIC

Exponential growth curves for all cultures were fit over about three or more generations of doubling by linear regression of log-OD values; steady state was not assumed until cultures underwent at least two generations of approximately constant exponential growth. When indicated, uncertainty in the calculated growth rate is SE of the resultant slope from the simple linear regression. A growth rate of zero indicates that cultures failed to grow after at least 12 hours or stopped growing within several doublings after addition of antibiotic (for example, see black triangles in fig. S11). If results were ambiguous at a particular Cm concentration, for example, if a culture appeared not to grow for 6 hours and then exhibited fast growth (which occurred rarely), the experiment was repeated in full. For Cm- and Tc-resistant strains, we determined MIC by monitoring the OD of batch cultures as described above (see Fig. 3, B and C, and fig. S11); we determined that cultures contained [Cm] ≥ MIC if cultures failed to grow or if growth rate $\lambda \leq 0.1$ hour^{-1}. For strains with high levels of antibiotic resistance (most strains), MIC was unambiguous in that growth was undetectable above some threshold concentration (see, for example, fig. S11). We first determined MICs with antibiotic concentrations set at logarithmic intervals before using finer gradations at linear intervals to achieve a determination within ~10% error. Because our quantitative model is formulated on the basis of growth in batch cultures, we use these MICs determined in batch cultures wherever we provide model predictions or fits. Additionally, the MIC determined on agar plates (called MIC_{plate}, see figs. S2 and S13 and methods below) and in the microfluidic device (Fig. 2, C and D) generally agreed with these determinations.

Growth of Colonies on Agar Plates

Determining CFU on Plates with Cm

For each strain, cells from log-phase batch cultures grown in minimal medium lacking Cm were diluted with the same medium. We then used sterile glass beads (Kimble, 4 mm) to spread 50 µl of the diluted culture onto an LB-Cm agar plate to achieve a density of several hundred cells per plate (giving rise to several hundred colonies or fewer after incubation, depending on the strain's response to the particular Cm concentration used). Plates were incubated overnight (~18 hours) at 37°C such that colonies formed were easily resolved by the naked eye (see fig. S2, B and C, and Fig. 3B). We used Bio-Rad Gel Doc XR and Quantity One software to photograph plates and count colonies; in many cases, colonies were also counted manually. We calibrated the counting software to agree with manual counts. Plate images were enhanced for brightness and contrast.

Determination of MIC_{plate}

Similar to above, cells were diluted from log phase in the absence of antibiotics, and 50 µl of diluted culture were spread onto LB-Cm agar plates to achieve a density of about 5×10^4 to 8×10^4 cells per plate before incubation. Plates were incubated overnight (~18 hours) at 37°C to reveal colony formation. MIC_{plate} is taken as the Cm concentration above which colonies appeared at a frequency of less than $\sim 10^{-4}$ per inoculant; the presence or absence of colony growth was readily visually discernable (figs. S2, S3, and S14). We determined MIC_{plate} values for each strain after at least two replicate experiments, and plate images were enhanced for brightness and contrast. These MIC_{plate} values obtained with LB plates for antibiotic-resistant strains were similar to MIC values obtained in batch cultures with minimal media as described above. Coincidence between MIC determined in LB and minimal media has been reported elsewhere (*43*).

Viability After Amp Enrichment Assays

Cells from overnight batch cultures in drug-free minimal media were diluted into the same fresh media with the indicated concentration of "drug" (Cm or Mn as designated in the text) and incubated for 1 to 2 hours. Cultures were then diluted in identical medium (containing Cm or Mn) with further addition of Amp (100 µg/ml) to an OD_{600} of about 1×10^{-3} to 2×10^{-3}. At this time, 50-µl aliquots of culture and 100-fold diluted culture were spread onto LB agar plates lacking any antibiotics and incubated overnight, producing plates containing ~500 and $\sim 5\times 10^4$ colonies each. These plates served as a control to monitor CFU at the start of enrichment and allowed us to determine the fraction of cells killed by the enrichment procedure at each drug concentration. After 6 to 7 hours of enrichment in drug and Amp media, 50-µl aliquots of culture and 100-fold diluted culture were again spread onto LB plates without antibiotics for overnight incubation; see fig. S5 for illustration. All plates and batch cultures were incubated at 37°C. Plate images were enhanced for brightness and contrast (figs. S7, S13, and S15).

Microfluidic Experiments

Cell Growth in Microfluidic Chambers

All cultures were grown at 37°C. The growth medium was minimal medium, as described above, and was filtered through 0.45-µm filters before use. The cells were first cultured in LB broth in 20-mm test tubes with shaking (250 rpm) in a water bath (New Brunswick Scientific). After 5 to 6 hours of growth, they were transferred to the growth medium and grew overnight in the same condition (preculture). The preculture was inoculated with fewer than 10^5 cells/ml so that cells were in an exponential phase at the time of experiment. The next morning, the preculture was diluted in fresh growth medium containing 0.1% BSA (bovine serum albumin; Sigma; BSA prevents cells from binding to surfaces of microfluidic devices) to an OD_{600} of ~0.01 as measured on a Genesys 20 spectrophotometer (Thermo Fisher) with the standard cuvette (16.100-Q-10/Z8.5, Starna Cells Inc.; ~200 µl per measurement). To load cells into the microfluidic device, the diluted preculture was pressurized to 1 to 2 psi at the outlet of the device (fig. S4A). When the channel and growth chambers were completely filled with the preculture, the preculture source was removed, and fresh growth medium was introduced from the inlet of the device.

The microfluidic device was fixed onto a motorized microscope stage equipped with autofocus (ProScan II, Prior) in a fluorescence microscope (Nikon TI-U) that was housed in a microscope incubator (InVivo Scientific). When viewed with a charge-coupled device (CCD) camera (Clara, Andor) with a 60× phase-contrast objective, single cells were dispersed far from each other (more than 100 µm away from each other). Then, −0.5 to −1.5 psi of vacuum were applied from the outlet to bring down the ceiling of the growth chambers and loosely sandwich the cells in place (side view of fig. S4). Because the vacuum induces the fresh medium flow in a channel (flow rate of 50 to 100 µm/s), no additional pressure was applied from the inlet.

After about two generations of unperturbed growth at 37°C in the device, we gently flushed excess cells away to prevent crowding and enable cell tracking, and then introduced growth medium with various concentrations of Cm to the inlet of the device. The 10 to 30 positions that contained a single microcolony in the view (~100 µm × ~100 µm) of the CCD were saved in the motorized stage. Phase-contrast images of the growing cells for each position were recorded two times per doubling. Fluorescence images were taken once per doubling, immediately after the phase-contrast images for each position with a Xenon excitation lamp (Sutter Instrument). The images were analyzed with a custom-built Matlab program. First, the program identified pixel positions occupied by cells with phase-contrast images, obtained the size of a growing colony in time series for each position, and calculated the growth rate of the colony. To quantify fluorescence levels, fluorescence intensities over the cell-occupying area identified by phase-contrast images were averaged.

Enriching Cm-Resistant Cells with Amp in Microfluidic Chambers

First, cells that constitutively express green fluorescent protein (GCat1m) were transferred from precultures as described above and grown in medium with 0.7 mM Cm for 8 hours. Initially, 44% of cells grew with a doubling time of 130 min, which is similar to the growth of Cat1m (Fig. 2C). We added Amp (200 µg/ml) to the medium at $t = 9$ hours to kill growing cells (fig. S6). At $t = 24$ hours, all growing cells had stopped growing and lost fluorescence. There were several nongrowing cells that maintained green fluorescence. At $t = 25$ hours, Cm and Amp were removed from the medium. Between $33 \le t \le 37$ hours, the nongrowing cells that maintained their fluorescence throughout the enrichment resumed growth.

Additional Protocols

Details regarding strain construction, microfluidic device fabrication, CAT, and β-galactosidase assays are described elsewhere (*40*).

References and Notes

1. A. J. Alanis, Resistance to antibiotics: Are we in the post-antibiotic era? *Arch. Med. Res.* **36**, 697–705 (2005). doi: 10.1016/j.arcmed.2005.06.009; pmid: 16216651
2. World Health Organization, *The Evolving Threat of Antimicrobial Resistance: Options for Action* (World Health Organization, Geneva, 2012).
3. J. L. Martínez, F. Baquero, D. I. Andersson, Predicting antibiotic resistance. *Nat. Rev. Microbiol.* **5**, 958–965 (2007). doi: 10.1038/nrmicro1796; pmid: 18007678
4. R. C. MacLean, A. R. Hall, G. G. Perron, A. Buckling, The population genetics of antibiotic resistance: Integrating molecular mechanisms and treatment contexts. *Nat. Rev. Genet.* **11**, 405–414 (2010). doi: 10.1038/nrg2778; pmid: 20479772
5. A. G. McArthur *et al.*, The comprehensive antibiotic resistance database. *Antimicrob. Agents Chemother.* **57**, 3348–3357 (2013). doi: 10.1128/AAC.00419-13; pmid: 23650175
6. L. L. Cavalli, G. A. Maccacaro, Chloromycetin resistance in *E. coli*, a case of quantitative inheritance in bacteria. *Nature* **166**, 991–992 (1950). doi: 10.1038/166991a0; pmid: 14796661
7. E. Toprak *et al.*, Evolutionary paths to antibiotic resistance under dynamically sustained drug selection. *Nat. Genet.* **44**, 101–105 (2011). doi: 10.1038/ng.1034; pmid: 22179135
8. D. J. Maskell, C. E. Hormaeche, K. A. Harrington, H. S. Joysey, F. Y. Liew, The initial suppression of bacterial growth in a salmonella infection is mediated by a localized rather than a systemic response. *Microb. Pathog.* **2**, 295–305 (1987). doi: 10.1016/0882-4010(87)90127-6; pmid: 3333801
9. J. C. Batten, R. M. McCune Jr., The influence of corticotrophin and certain corticosteroids on populations of *Mycobacterium tuberculosis* in tissues of mice. *Br. J. Exp. Pathol.* **38**, 413–423 (1957). pmid: 13460186
10. Y. Li, A. Karlin, J. D. Loike, S. C. Silverstein, A critical concentration of neutrophils is required for effective bacterial killing in suspension. *Proc. Natl. Acad. Sci. U.S.A.* **99**, 8289–8294 (2002). doi: 10.1073/pnas.122244799; pmid: 12060772
11. R. Malka, B. Wolach, R. Gavrieli, E. Shochat, V. Rom-Kedar, Evidence for bistable bacteria-neutrophil interaction and its clinical implications. *J. Clin. Invest.* **122**, 3002–3011 (2012). doi: 10.1172/JCI59832; pmid: 22820292
12. J. A. Washington II, The effects and significance of subminimal inhibitory concentrations of antibiotics. *Rev. Infect. Dis.* **1**, 781–786 (1979). doi: 10.1093/clinids/1.5.781; pmid: 396633
13. J. Davies, G. B. Spiegelman, G. Yim, The world of subinhibitory antibiotic concentrations. *Curr. Opin. Microbiol.* **9**, 445–453 (2006). doi: 10.1016/j.mib.2006.08.006; pmid: 16942902
14. C. Tan, P. Marguet, L. You, Emergent bistability by a growth-modulating positive feedback circuit. *Nat. Chem. Biol.* **5**, 842–848 (2009). doi: 10.1038/nchembio.218; pmid: 19801994
15. A. Zaslaver *et al.*, Invariant distribution of promoter activities in *Escherichia coli*. *PLOS Comput. Biol.* **5**, e1000545 (2009). doi: 10.1371/journal.pcbi.1000545; pmid: 19851443
16. M. Scott, C. W. Gunderson, E. M. Mateescu, Z. Zhang, T. Hwa, Interdependence of cell growth and gene expression: Origins and consequences. *Science* **330**, 1099–1102 (2010). doi: 10.1126/science.1192588; pmid: 21097934
17. T. Bollenbach, R. Kishony, Resolution of gene regulatory conflicts caused by combinations of antibiotics. *Mol. Cell* **42**, 413–425 (2011). doi: 10.1016/j.molcel.2011.04.016; pmid: 21596308

18. M. Scott, T. Hwa, Bacterial growth laws and their applications. *Curr. Opin. Biotechnol.* **22**, 559–565 (2011). doi: 10.1016/j.copbio.2011.04.014; pmid: 21592775
19. D. Dubnau, R. Losick, Bistability in bacteria. *Mol. Microbiol.* **61**, 564–572 (2006). doi: 10.1111/j.1365-2958.2006.05249.x; pmid: 16879639
20. W. K. Smits, O. P. Kuipers, J. W. Veening, Phenotypic variation in bacteria: The role of feedback regulation. *Nat. Rev. Microbiol.* **4**, 259–271 (2006). doi: 10.1038/nrmicro1381; pmid: 16541134
21. J. M. Andrews, Determination of minimum inhibitory concentrations. *J. Antimicrob. Chemother.* **48** (suppl. 1), 5–16 (2001). doi: 10.1093/jac/48.suppl_1.5; pmid: 11420333
22. R. J. Harvey, A. L. Koch, How partially inhibitory concentrations of chloramphenicol affect the growth of *Escherichia coli*. *Antimicrob. Agents Chemother.* **18**, 323–337 (1980). doi: 10.1128/AAC.18.2.323; pmid: 6160809
23. J. Ellis, C. R. Bagshaw, W. Shaw, Kinetic mechanism of chloramphenicol acetyltransferase: The role of ternary complex interconversion in rate determination. *Biochemistry* **34**, 16852–16859 (1995). doi: 10.1021/bi00051a036; pmid: 8527461
24. W. V. Shaw, Chloramphenicol acetyltransferase: Enzymology and molecular biology. *CRC Crit. Rev. Biochem.* **14**, 1–46 (1983). doi: 10.3109/10409238309102789; pmid: 6340955
25. H. Harbottle, S. Thakur, S. Zhao, D. G. White, Genetics of antimicrobial resistance. *Anim. Biotechnol.* **17**, 111–124 (2006). doi: 10.1080/10495390600957092; pmid: 17127523
26. T. J. Foster, Plasmid-determined resistance to antimicrobial drugs and toxic metal ions in bacteria. *Microbiol. Rev.* **47**, 361–409 (1983). pmid: 6355806
27. L. J. Piddock, Clinically relevant chromosomally encoded multidrug resistance efflux pumps in bacteria. *Clin. Microbiol. Rev.* **19**, 382–402 (2006). doi: 10.1128/CMR.19.2.382-402.2006; pmid: 16614254
28. A. Groisman *et al.*, A microfluidic chemostat for experiments with bacterial and yeast cells. *Nat. Methods* **2**, 685–689 (2005). doi: 10.1038/nmeth784; pmid: 16118639
29. J. J. Rahal Jr., M. S. Simberkoff, Bactericidal and bacteriostatic action of chloramphenicol against meningeal pathogens. *Antimicrob. Agents Chemother.* **16**, 13–18 (1979). doi: 10.1128/AAC.16.1.13; pmid: 38742
30. J. Bigger, Treatment of staphylococcal infections with penicillin by intermittent sterilisation. *Lancet* **244**, 497–500 (1944). doi: 10.1016/S0140-6736(00)74210-3
31. N. Q. Balaban, J. Merrin, R. Chait, L. Kowalik, S. Leibler, Bacterial persistence as a phenotypic switch. *Science* **305**, 1622–1625 (2004). doi: 10.1126/science.1099390; pmid: 15308767
32. K. Lewis, Persister cells, dormancy and infectious disease. *Nat. Rev. Microbiol.* **5**, 48–56 (2007). doi: 10.1038/nrmicro1557; pmid: 17143318
33. K. Gerdes, E. Maisonneuve, Bacterial persistence and toxin-antitoxin loci. *Annu. Rev. Microbiol.* **66**, 103–123 (2012). doi: 10.1146/annurev-micro-092611-150159; pmid: 22994490
34. H. G. Schlegel, H. W. Jannasch, Enrichment cultures. *Annu. Rev. Microbiol.* **21**, 49–70 (1967). doi: 10.1146/annurev.mi.21.100167.000405; pmid: 4860267
35. R. M. Cozens *et al.*, Evaluation of the bactericidal activity of β-lactam antibiotics on slowly growing bacteria cultured in the chemostat. *Antimicrob. Agents Chemother.* **29**, 797–802 (1986). doi: 10.1128/AAC.29.5.797; pmid: 3089141
36. E. Jawetz, J. B. Gunnison, R. S. Speck, V. R. Coleman, Studies on antibiotic synergism and antagonism: The interference of chloramphenicol with the action of penicillin. *AMA Arch. Intern. Med.* **87**, 349–359 (1951). doi: 10.1001/archinte.1951.03810030022002; pmid: 14810260
37. S. E. Holm, Interaction between β-lactam and other antibiotics. *Rev. Infect. Dis.* **8** (suppl. 3), S305–S314 (1986). doi: 10.1093/clinids/8.Supplement_3.S305; pmid: 3529323
38. D. Schnappinger, W. Hillen, Tetracyclines: Antibiotic action, uptake, and resistance mechanisms. *Arch. Microbiol.* **165**, 359–369 (1996). doi: 10.1007/s002030050339; pmid: 8661929
39. I. Chopra, M. Roberts, Tetracycline antibiotics: Mode of action, applications, molecular biology, and epidemiology of bacterial resistance. *Microbiol. Mol. Biol. Rev.* **65**, 232–260 (2001). doi: 10.1128/MMBR.65.2.232-260.2001; pmid: 11381101
40. See supporting materials and methods in *Science* Online.
41. L. M. McMurry, A. M. George, S. B. Levy, Active efflux of chloramphenicol in susceptible *Escherichia coli* strains and in multiple-antibiotic-resistant (Mar) mutants. *Antimicrob. Agents Chemother.* **38**, 542–546 (1994). doi: 10.1128/AAC.38.3.542; pmid: 8203852
42. Here and elsewhere in the text, "expression level" denotes the intracellular concentration of a protein. This is reported in units of protein activity per OD: Protein activity is proportional to the protein amount. OD units correspond reliably to cell volume (*57*, *67*, *68*).
43. T. Bollenbach, S. Quan, R. Chait, R. Kishony, Nonoptimal microbial response to antibiotics underlies suppressive drug interactions. *Cell* **139**, 707–718 (2009). doi: 10.1016/j.cell.2009.10.025; pmid: 19914165
44. O. Maaløe, in *Biological Regulation and Development*, R. F. Goldberger, Ed. (Plenum Press, New York, 1979), pp. 487–542.
45. R. Hermsen, J. B. Deris, T. Hwa, On the rapidity of antibiotic resistance evolution facilitated by a concentration gradient. *Proc. Natl. Acad. Sci. U.S.A.* **109**, 10775–10780 (2012). doi: 10.1073/pnas.1117716109; pmid: 22711808
46. Q. Zhang *et al.*, Acceleration of emergence of bacterial antibiotic resistance in connected microenvironments. *Science* **333**, 1764–1767 (2011). doi: 10.1126/science.1208747; pmid: 21940899
47. P. Greulich, B. Waclaw, R. J. Allen, Mutational pathway determines whether drug gradients accelerate evolution of drug-resistant cells. *Phys. Rev. Lett.* **109**, 088101 (2012). doi: 10.1103/PhysRevLett.109.088101; pmid: 23002776
48. M. E. Falagas, A. P. Grammatikos, A. Michalopoulos, Potential of old-generation antibiotics to address current need for new antibiotics. *Expert Rev. Anti Infect. Ther.* **6**, 593–600 (2008). doi: 10.1586/14787210.6.5.593; pmid: 18847400
49. Y. Hayashi, D. L. Paterson, The epidemiology of pan/extreme drug resistance, in *Antibiotic Policies*, I. M. Gould, J. W. M. van der Meer, Eds. (Springer, New York, 2011), pp. 27–38.
50. T. Nichterlein *et al.*, Subinhibitory concentrations of β-lactams and other cell-wall antibiotics inhibit listeriolysin production by *Listeria monocytogenes*. *Int. J. Antimicrob. Agents* **7**, 75–81 (1996). doi: 10.1016/0924-8579(96)00014-3; pmid: 18611740
51. M. Niewerth *et al.*, Ciclopirox olamine treatment affects the expression pattern of *Candida albicans* genes encoding virulence factors, iron metabolism proteins, and drug resistance. *Antimicrob. Agents Chemother.* **47**, 1805–1817 (2003). doi: 10.1128/AAC.47.6.1805-1817.2003; pmid: 12760852
52. D. I. Andersson, D. Hughes, Antibiotic resistance and its cost: Is it possible to reverse resistance? *Nat. Rev. Microbiol.* **8**, 260–271 (2010). pmid: 20208551
53. E. Gullberg *et al.*, Selection of resistant bacteria at very low antibiotic concentrations. *PLOS Pathog.* **7**, e1002158 (2011). doi: 10.1371/journal.ppat.1002158; pmid: 21811410
54. J. Elf, K. Nilsson, T. Tenson, M. Ehrenberg, Bistable bacterial growth rate in response to antibiotics with low membrane permeability. *Phys. Rev. Lett.* **97**, 258104 (2006). doi: 10.1103/PhysRevLett.97.258104; pmid: 17280399
55. C. Tan *et al.*, The inoculum effect and band-pass bacterial response to periodic antibiotic treatment. *Mol. Syst. Biol.* **8**, 617 (2012). doi: 10.1038/msb.2012.49; pmid: 23047527
56. M. A. Kohanski, D. J. Dwyer, B. Hayete, C. A. Lawrence, J. J. Collins, A common mechanism of cellular death induced by bactericidal antibiotics. *Cell* **130**, 797–810 (2007). doi: 10.1016/j.cell.2007.06.049; pmid: 17803904
57. S. Klumpp, Z. Zhang, T. Hwa, Growth rate-dependent global effects on gene expression in bacteria. *Cell* **139**, 1366–1375 (2009). doi: 10.1016/j.cell.2009.12.001; pmid: 20064380
58. R. A. Fasani, M. A. Savageau, Molecular mechanisms of multiple toxin–antitoxin systems are coordinated to govern the persister phenotype. *Proc. Natl. Acad. Sci. U.S.A.* **110**, E2528–E2537 (2013). doi: 10.1073/pnas.1301023110; pmid: 23781105
59. C. Lou, Z. Li, Q. Ouyang, A molecular model for persister in *E. coli*. *J. Theor. Biol.* **255**, 205–209 (2008). doi: 10.1016/j.jtbi.2008.07.035; pmid: 18721814
60. C. You *et al.*, Coordination of bacterial proteome with metabolism by cyclic AMP signalling. *Nature* **500**, 301–306 (2013). doi: 10.1038/nature12446; pmid: 23925119
61. J. J. Snell, D. F. Brown, External quality assessment of antimicrobial susceptibility testing in Europe. *J. Antimicrob. Chemother.* **47**, 801–810 (2001). doi: 10.1093/jac/47.6.801; pmid: 11389112
62. P. E. Varaldo, Antimicrobial resistance and susceptibility testing: An evergreen topic. *J. Antimicrob. Chemother.* **50**, 1–4 (2002). doi: 10.1093/jac/dkf093; pmid: 12095999
63. J. B. Michel, P. J. Yeh, R. Chait, R. C. Moellering Jr., R. Kishony, Drug interactions modulate the potential for evolution of resistance. *Proc. Natl. Acad. Sci. U.S.A.* **105**, 14918–14923 (2008). doi: 10.1073/pnas.0800944105; pmid: 18815368
64. L. N. Csonka, T. P. Ikeda, S. A. Fletcher, S. Kustu, The accumulation of glutamate is necessary for optimal growth of *Salmonella typhimurium* in media of high osmolality but not induction of the proU operon. *J. Bacteriol.* **176**, 6324–6333 (1994). pmid: 7929004
65. K. A. Loftin, C. D. Adams, M. T. Meyer, R. Surampalli, Effects of ionic strength, temperature, and pH on degradation of selected antibiotics. *J. Environ. Qual.* **37**, 378–386 (2008). doi: 10.2134/jeq2007.0230; pmid: 18268300
66. T. Stoichev, M. S. Baptista, M. C. P. Basto, V. M. Vasconcelos, M. T. S. D. Vasconcelos, Effects of minocycline and its degradation products on the growth of *Microcystis aeruginosa*. *Ecotoxicol. Environ. Saf.* **74**, 219–224 (2011). doi: 10.1016/j.ecoenv.2010.10.015; pmid: 20965566
67. W. Donachie, A. Robinson, in Escherichia coli and Salmonella typhimurium: *Cellular and Molecular Biology*, F. C. Neidhardt *et al.*, Eds. (American Society for Microbiology, Washington, DC, 1987), pp. 1578–1592.
68. H. E. Kubitschek, W. W. Baldwin, S. J. Schroeter, R. Graetzer, Independence of buoyant cell density and growth rate in *Escherichia coli*. *J. Bacteriol.* **158**, 296–299 (1984). pmid: 6370960
69. L. Sandegren, D. I. Andersson, Bacterial gene amplification: Implications for the evolution of antibiotic resistance. *Nat. Rev. Microbiol.* **7**, 578–588 (2009). doi: 10.1038/nrmicro2174; pmid: 19609259
70. R. Hermsen, T. Hwa, Sources and sinks: A stochastic model of evolution in heterogeneous environments. *Phys. Rev. Lett.* **105**, 248104 (2010). doi: 10.1103/PhysRevLett.105.248104; pmid: 21231560

Acknowledgments: We are grateful to R. Austin, L. Chao, M. Ehrenberg, P. Geiduschek, H. Nikaido, S. Klumpp, M. Scott, B. Shaw, Q. Zhang, and members of the Hwa laboratory for comments and suggestions. This work was supported by the NIH through grant R01-GM095903 to T.H., by the NSF, through an NSF Graduate Research Fellowship to J.B.D. and through the Center for Theoretical Biological Physics (PHY0822283), and by the National Cancer Institute via a subcontract of the Physical Science-Oncology program (1 U54 CA143803). R.H. was supported in part by the NWO (Nederlandse Organisatie voor Wetenschappelijk Onderzoek) (VENI 680-47-419). Additional data, including source data for figures, are presented in the supplementary materials. Correspondence and requests for materials should be addressed to T.H. (hwa@ucsd.edu).

Supplementary Materials

www.sciencemag.org/content/342/6162/1237435/suppl/DC1
Materials and Methods
Figs. S1 to S19
Tables S1 to S5
References (*71*–*121*)
Movies S1 and S2

10.1126/science.1237435